JOURNAL OF GEOPHYSICAL RESEARCH, VOL. 114, D06201, doi:10.1029/2008JD010451, 2009

Scattering database in the millimeter and submillimeter wave range of 100–1000 GHz for nonspherical ice particles

Gang Hong,[1] Ping Yang,[1] Bryan A. Baum,[2] Andrew J. Heymsfield,[3] Fuzhong Weng,[4] Quanhua Liu,[5,6] Georg Heygster,[7] and Stefan A. Buehler[8]

Received 19 May 2008; revised 21 October 2008; accepted 2 January 2009; published 17 March 2009.

[1] The inference of ice cloud properties from spaceborne sensors is sensitive to the retrieval algorithms and satellite sensors used. To approach a better understanding of ice cloud properties, it is necessary to combine satellite measurements from multiple platforms and sensors operating in visible, infrared, and millimeter and submillimeter-wave regions of the electromagnetic spectrum. The single-scattering properties of ice particles with consistent ice particle models are the basis for estimating the optical and microphysical properties of ice clouds from multiple satellite sensors. In this study, the single-scattering properties (extinction efficiency, absorption efficiency, single-scattering albedo, asymmetry factor, and scattering phase matrix) of nonspherical ice particles, assumed to be hexagonal solid and hollow columns, hexagonal plates, 3D bullet rosettes, aggregates, and droxtals, are computed from the discrete dipole approximation method for 21 millimeter and submillimeter-wave frequencies ranging from 100 to 1000 GHz. A database of the single-scattering properties of nonspherical ice particles are developed for 38 particle sizes ranging from 2 to 2000 μm in terms of particle maximum dimension. The bulk scattering properties of ice clouds consisting of various ice particles, which are the fundamental to the radiative transfer in ice clouds, are developed on the basis of a set of 1119 particle size distributions obtained from various field campaigns.

Citation: Hong, G., P. Yang, B. A. Baum, A. J. Heymsfield, F. Weng, Q. Liu, G. Heygster, and S. A. Buehler (2009), Scattering database in the millimeter and submillimeter wave range of 100–1000 GHz for nonspherical ice particles, *J. Geophys. Res.*, *114*, D06201, doi:10.1029/2008JD010451.

1. Introduction

[2] The inference of ice cloud properties on a global scale is achieved operationally through analysis of passive satellite imager data, such as from the Moderate Resolution Imaging Spectroradiometer [MODIS, *Platnick et al.*, 2003; *King et al.*, 2003, 2006; *Menzel et al.*, 2008]. Recent studies indicate that an important complement to the imager data is available from hyperspectral infrared (IR) data provided by infrared sounders such as the Atmospheric Infrared Sounder [AIRS, *Huang et al.*, 2004; *Li et al.*, 2005; *Kahn et al.*, 2007]. Moreover, measurements at microwave frequencies (millimeter and submillimeter-waves) have been suggested to complement the retrievals of the microphysical and optical properties of ice cloud from visible and infrared measurements [e.g., *Wang et al.*, 2001; *Miao et al.*, 2003; *Evans et al.*, 2005; *Wu et al.*, 2006; *Buehler et al.*, 2007; *Weinman and Kim*, 2007; *Hong et al.*, 2008a, 2008b].

[3] It is unlikely possible to gain any new insight into the relationship between the retrievals from these different sensors if the single-scattering properties of the ice particle models used in the retrieval process were derived inconsistently. New ice cloud bulk scattering models have been derived for imagers, such as MODIS [*Baum et al.*, 2005a, 2005b]. These models are now used for MODIS Collection 5 products [*King et al.*, 2004, 2006]. Models were developed using similar methodology for hyperspectral sounder, such as AIRS [*Baum et al.*, 2007] based on the single-scattering property database reported in *Yang et al.* [2005]. These models are based on a mixture of nonspherical ice particles including hexagonal solid and hollow columns, hexagonal plates, 3D bullet rosettes, aggregates, and droxtals [*Yang et al.*, 2000, 2005]. What is still needed is a full set of single-scattering properties at appropriate millimeter and submillimeter wavelengths for this same set of ice particles. The purpose of this study is to provide information regarding the development of such a database of single-

[1] Department of Atmospheric Sciences, Texas A&M University, College Station, Texas, USA.
[2] Space Science and Engineering Center, University of Wisconsin, Madison, Wisconsin, USA.
[3] National Center for Atmospheric Research, Boulder, Colorado, USA.
[4] Satellite Meteorology and Climatology Division, Center for Satellite Applications and Research, NOAA NESDIS, Camp Springs, Maryland, USA.
[5] Joint Center for Satellite Data Assimilation, NOAA NESDIS, Camp Springs, Maryland, USA.
[6] QSS Group, Incorporated, Camp Springs, Maryland, USA.
[7] Institute of Environmental Physics, University of Bremen, Bremen, Germany.
[8] Department of Space Science, Lulea University of Technology, Kiruna, Sweden.

0148-0227/09/2008JD010451$09.00

scattering properties for the same ice particles as those reported in earlier studies.

[4] *Evans and Stephens* [1995] computed microwave single-scattering properties of solid and hollow columns, hexagonal plates, and planar bullet rosettes at the frequencies of 85–340 GHz. This study was extended to the frequencies up to 880 GHz by *Evans et al.* [1998]. *Czekala and Simmer* [1998] and *Czekala et al.* [1999] investigated the sensitivity of microwave radiative transfer to nonspherical precipitating hydrometeors at the range of 19–85 GHz. *Tang and Aydin* [1995] and *Aydin and Walsh* [1999] investigated the microwave scattering from spatial and planar bullet rosettes at 35, 94, and 220 GHz frequencies. *Liu* [2004] and *Kim* [2006] parameterized microwave single-scattering properties of precipitation-sized ice and snow particles at the frequencies of 89–340 GHz as a function of particle size. *Hong* [2007a] parameterized the bulk scattering properties as a function of ice cloud effective particle size at frequencies ranging between 89–340 GHz, assuming habit mixtures of hexagonal solid and hollow columns, hexagonal plates, 3D bullet rosettes, aggregates, and droxtals. *Hong* [2007b] investigated the development and use of similar models at 94 GHz for CloudSat. Recently, *Liu* [2008] developed a database containing the scattering properties for 11 ice particle habits at frequencies from 15 to 340 GHz. Among these databases and parameterizations for microwave scattering, *Tang and Aydin* [1995] and *Aydin and Walsh* [1999] focused on radar backscattering properties. *Kim* [2006], *Liu* [2004, 2008], *Czekala and Simmer* [1998], and *Czekala et al.* [1999] mainly focused on precipitation hydrometeors, while *Evans and Stephens* [1995], *Evans et al.* [1998] and *Hong* [2007a, 2007b] mainly focused on ice clouds.

[5] It is now necessary to extend the existing set of ice single-scattering properties to higher frequencies. Measurements at frequencies up to 640 GHz have been obtained from both satellite and aircraft sensors [e.g., *Wang et al.*, 2001; *Evans et al.*, 2005; *Weng et al.*, 2003; *Wu et al.*, 2006; *Eriksson et al.*, 2007]. Future satellite sensors have been suggested, which may include higher frequencies up to 900 GHz [e.g., *Evans et al.*, 2005; *Kunzi*, 2001; *Buehler et al.*, 2007].

[6] The intent of our effort is to build a complete scattering database of ice clouds for these millimeter and submillimeter waves, which are carried by current satellite and airborne sensors and by planned near future satellite sensors. This study extends the work of *Hong* [2007a] to 21 millimeter and submillimeter wave frequencies up to 1000 GHz covered by most current and planned satellite sensors or airborne sensors. The scattering database is for nonspherical ice particles that are consistent with those that have been used for the MODIS ice cloud retrievals. In addition to the single-scattering properties, such as the extinction and absorption efficiency, asymmetry parameter, and single-scattering albedo, we present results for the complete phase matrix and discuss the differences found between various nonspherical particles.

[7] The discrete-dipole approximation (DDA) method [*Draine and Flatau*, 1994] used for the present single-scattering properties, six nonspherical ice particle models, and particle size distributions of ice clouds from field measurements, are described in section 2. In section 3 the single-scattering properties of six nonspherical ice particles are computed using the DDA method first, and the bulk scattering properties of ice clouds composed of ice nonspherical particles are then derived by averaging the single-scattering properties of individual particles over measured particle size distributions of ice clouds. The conclusions of this study are given in section 4.

2. Models and Data

[8] Since the DDA method [*Draine and Flatau*, 1994; *Yurkin and Hoekstra*, 2007] has the greatest advantage of flexibly regarding ice particles with arbitrary geometries, it has been extensively used to compute the scattering properties of ice particles with complex habits [e.g., *Evans and Stephens*, 1995; *Lemke and Quante*, 1999; *Okamoto*, 2002; *Liu*, 2004, 2008; *Kim*, 2006; *Sato and Okamoto*, 2006; *Hong*, 2007a, 2007b]. In the DDA method, a scattering object is represented by a number of dipoles on a lattice with a given spacing between the individual dipoles. The space between the dipoles needs to be small in comparison with any structural lengths of the scattering object and the incident wavelength. The scattering properties of a scatterer (i.e., extinction efficiency, single-scattering albedo, and 4×4 scattering phase matrix) can be derived from the interaction between an array of dipoles and an incident monochromatic plane wave [*Purcell and Pennypacker*, 1973; *Draine and Flatau*, 2004]. In the DDSCAT, the definition of the Stokes vector (I, Q, U, V) (the sign of the power of e in the time dependent term is negative) follows that by *Bohren and Huffman* [1983]. The default result for Q_{ext} computed by the DDSCAT is the normalized extinction cross section by the projected area of a volume-equivalent sphere for the scatterer. In the present study, the Q_{ext} is the ratio of the extinction cross section to the projected area of the scatterer under random orientation conditions.

[9] Six nonspherical ice habits (hexagonal solid and hollow columns, hexagonal plates, 3D six-branch solid bullet rosettes, aggregates, and droxtals) are considered in this study. These same habits have been used for global retrievals of the optical and microphysical properties of ice clouds [e.g., *Platnick et al.*, 2003; *King et al.*, 2004, 2006; *Yang et al.*, 2005; *Baum et al.*, 2005a]. The geometry of each habit is discussed in detail by *Yang et al.* [2005] and *Hong* [2007a]. The detailed definitions of the six habits can be found in the Table 1 of *Hong* [2007a]. The ice refractive indices are taken from *Warren* [1984] at a temperature of -30°C (Figure 1). A set of 38 particle size bins, ranging from 2 to 2000 μm in maximum dimension D, are used for computing each particle's single-scattering properties.

[10] A conservative criterion with $|m|kd < 0.5$ (m is the complex refractive index of an ice particle and $k = 2\pi/\lambda$ is the wavenumber) is used for ensuring adequate DDA computations in this study [*Draine and Flatau*, 1994, 2004]. To ensure $|m|kd < 0.5$, the dipole numbers of ice particles vary with the particle size and frequency. The ice particles with the six nonspherical habits are assumed to be randomly oriented. The three orientation angles (β, θ, and ϕ) for averaging scattering quantity for the randomly oriented ice particles are in the ranges of 0°–360°, 0°–180°, and 0° –360°, respectively. Totally, 5600 orientations are considered for hexagonal columns, hollows, plates, and

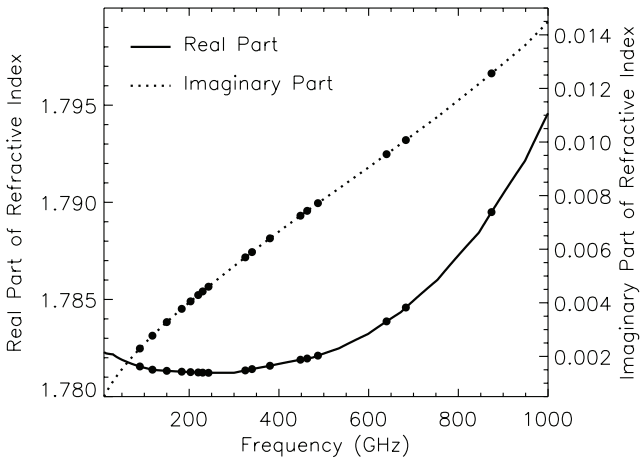

Figure 1. Refractive indices for millimeter and submillimeter waves ranging in 100–1000 GHz. The data are from *Warren* [1984] at a temperature of −30°C.

bullet rosettes, and 2160 orientations are used for droxtals. The total number of orientations are larger than the 1089 that were used by *Penttilä et al.* [2007] for their comparisons between discrete dipole implementations and exact techniques, which found that the DDSCAT produces accurate results. Aggregates use 750 orientations in order to save computation times. The total orientations for aggregates are adequate for the DDSCAT computations since the assumption of the habit of aggregates is arbitrary.

[11] The accuracy of the DDSCAT computations for scattering properties of ice particles at microwave frequencies has been investigated [*Evans and Stephens*, 1995; *Liu*, 2004, 2008; *Hong*, 2007a]. *Evans and Stephens* [1995] found that $|m|kd < 1$ can used be for reasonable accuracy (3%–12% RMS differences between the DDSCAT computations and exact techniques) and smaller $|m|kd$ is required for backscattering [*Hovenier et al.*, 1986; *Mishchenko and Hovenier*, 1995]. A more conservative criterion with $|m|kd < 0.5$ has been found to ensure the errors for microwave scattering properties of spheres on the basis of the DDSCAT are within 1% [*Liu*, 2004; *Hong*, 2007a]. *Penttilä et al.* [2007] investigated the accuracy of DDSCAT computations by comparing the results from Lorenz-Mie code for spheres and T-matrix for spheroids and cylinders. Two materials with refractive indices $1.6 + 0.001i$ (silicate) and $1.313 + 0i$ (ice) were used for their investigations. It was found that the relative accuracy for intensity is 2–6% and the absolute accuracy for linear polarization ratio is 1–3%.

[12] The real part of the refractive index of ice at microwave frequencies is higher than those used in *Penttilä et al.* [2007]. *Yurkin et al.* [2007a] compared the DDA and the FDTD method for simulating scattering properties of spheres in a range of size parameters up to 80 and real parts of refractive indices up to 2. The errors of the phase functions and linear polarization ratios from the DDA with respect to the Lorenz-Mie results are much smaller than those from the FDTD method when scatterers have large real parts of refractive indices that are close to those of ice particles at microwave frequencies. We compare the extinction efficiency, single-scattering albedo, asymmetry factor, phase function (P_{11}), and linear polarization ratio ($-P_{12}/P_{11}$) from the DDSCAT to those from the T-matrix for a spheroid and a cylinder with an aspect ratio of 5 and a maximum dimension of 1000 μm at 640 GHz. The extinction efficiency, single-scattering albedo, and asymmetry factor from the two techniques are essentially the same, i.e., with relative differences less than 0.5%. Figure 2 shows the differences of the phase functions and linear polarization ratios. The relative differences of the phase functions between the results from the DDSCAT and the T-matrix are within 6%. The absolute differences of linear polarization ratios ($-P_{12}/P_{11} \times 100$) are within 7%. Both of the two differences show that the DDSCAT provides reasonable results for microwave scattering properties.

[13] The particle size distributions (PSDs) used in this study are based on in situ measurements obtained from five field campaigns (two tropical and three midlatitude locations). The two tropical campaigns were conducted in Kwajalein, Marshall Islands in 1999 under the auspices of the Tropical Rainfall Measuring Mission [*Stith et al.*, 2002, 2004], and the Cirrus Regional Study of Tropical Anvils and Cirrus Layers Florida Area Cirrus Experiment in 2002. The three midlatitude campaigns include the First ISCCP Regional Experiment (FIRE; ISCCP refers to the International Satellite Cloud Climatology Project) in Madison,

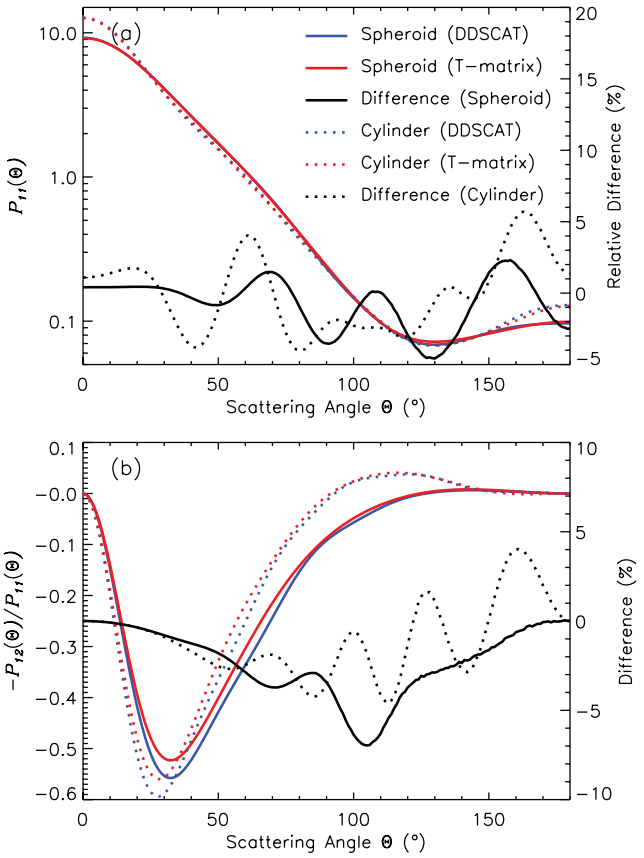

Figure 2. Comparisons of (a) phase functions and (b) linear polarization ratios from the DDSCAT to those from the T-matrix for a spheroid and a cylinder ice particles with an aspect ratio of 5 at 640 GHz.

Table 1. Satellite and Airborne Millimeter and Submillimeter Wave Sensors and Their Band Center Frequencies Included in the Present Database[a]

Acronym	Sensor Name and Platform	Center Frequency (GHz)	Reference
AMSU-B	Advanced Microwave Sounding Unit-B, NOAA	89, 150, 183	*Saunders et al.* [1995]
HSB	Humidity Sounder for Brazil, Aqua	89, 150, 183	*Aumann et al.* [2003]
SSM/T2	Special Sensor Microwave Temperature-2, Defense Meteorological Satellite Program	89, 150, 183	*Falcone et al.* [1992]
SSMIS	Special Sensor Microwave Imager/Sounder, Defense Meteorological Satellite Program	89, 150, 183	*Bommarito* [1993]
UARS MLS	Microwave Limb Sounder, Upper Atmosphere Research Satellite	183, 205	*Wu et al.* [2005]
EOS MLS	Earth Observing System Microwave Limb Sounder, Aura	118, 190, 240, 640	*Wu et al.* [2006]
Odin-SMR	Sub-Millimeter Radiometer, Odin	118, 486–581 (500)	*Eriksson et al.* [2007]
MHS	Microwave Humidity Sounder, Meteorological Operational satellite programme-A	89, 157, 183, 190	*Arriaga* [2000]
SWCIR	Submillimeter-Wave Cloud Ice Radiometer, NASA DC-8	183, 325, 448, 643	*Evans et al.* [2002]
MIR	Millimeter-wave Imaging Radiometer, NASA ER-2	89, 150, 183, 220, 325, 340	*Wang et al.* [2001]
NAST-M	NPOESS Aircraft Sounder Testbed-Microwave, NASA ER-2	118, 183, 425	*Blackwell et al.* [2001]
HAMSR	High Altitude Monolithic Microwave Integrated Circuit Scanning Radiometer, NASA ER-2	166, 183	*Skofronick-Jackson et al.* [2008]
CoSSIR	Compact Scanning Submillimeter-wave Imaging Radiometer, NASA ER-2	183, 220, 380, 487, 640	*Evans et al.* [2005]
PSR-S	Polarimetric Scanning Radiometer/Sounding, NASA DC-8, ER-2, P3-B, Proteus, WB-57F	89, 118, 183, 325, 340, 380, 425, 500	*Piepmeier and Gasiewski* [1996]
GPM-GMI[b]	Global Precipitation Measurement Microwave Imager, Global Precipitation Measurement	89, 166, 183	*Bidwell et al.* [2005]
ATMS[b]	Advanced Technology Microwave Sounder, NPOESS	87–91 (89), 164–167 (166), 183	*Muth et al.* [2004]
CMIS[b]	Conical Microwave Imager/Sounder, NPOESS	89, 166, 183	*Chauhan et al.* [2005]
MWRI[b]	Microwave Radiation Imager, FengYun-3	89, 150	*Zhang et al.* [2006]
MWHS[b]	MicroWave Humidity Sounder, FengYun-3	150, 183	*Zhang et al.* [2006]
MADRAS[b]	Microwave Analysis and Detection of Rain and Atmospheric Structures, Megha-Tropiques	89, 157	*Desbois et al.* [2003]
SAPHIR[b]	Sounder for Atmospheric Profiling of Humidity in the Intertropics by Radiometry, Megha-Tropiques	183	*Desbois et al.* [2003]
CIWSIR[b]	Cloud Ice Water Submillimeter Imaging Radiometer	150, 183, 220, 243, 325, 462, 664, 683, 874[c]	*Buehler et al.* [2007]

[a]The frequencies in the brackets are chosen for the corresponding frequency ranges.
[b]Planned near future sensors.
[c]Some channels are no longer included in the latest instrument concept, but it is still of interest for simulations.

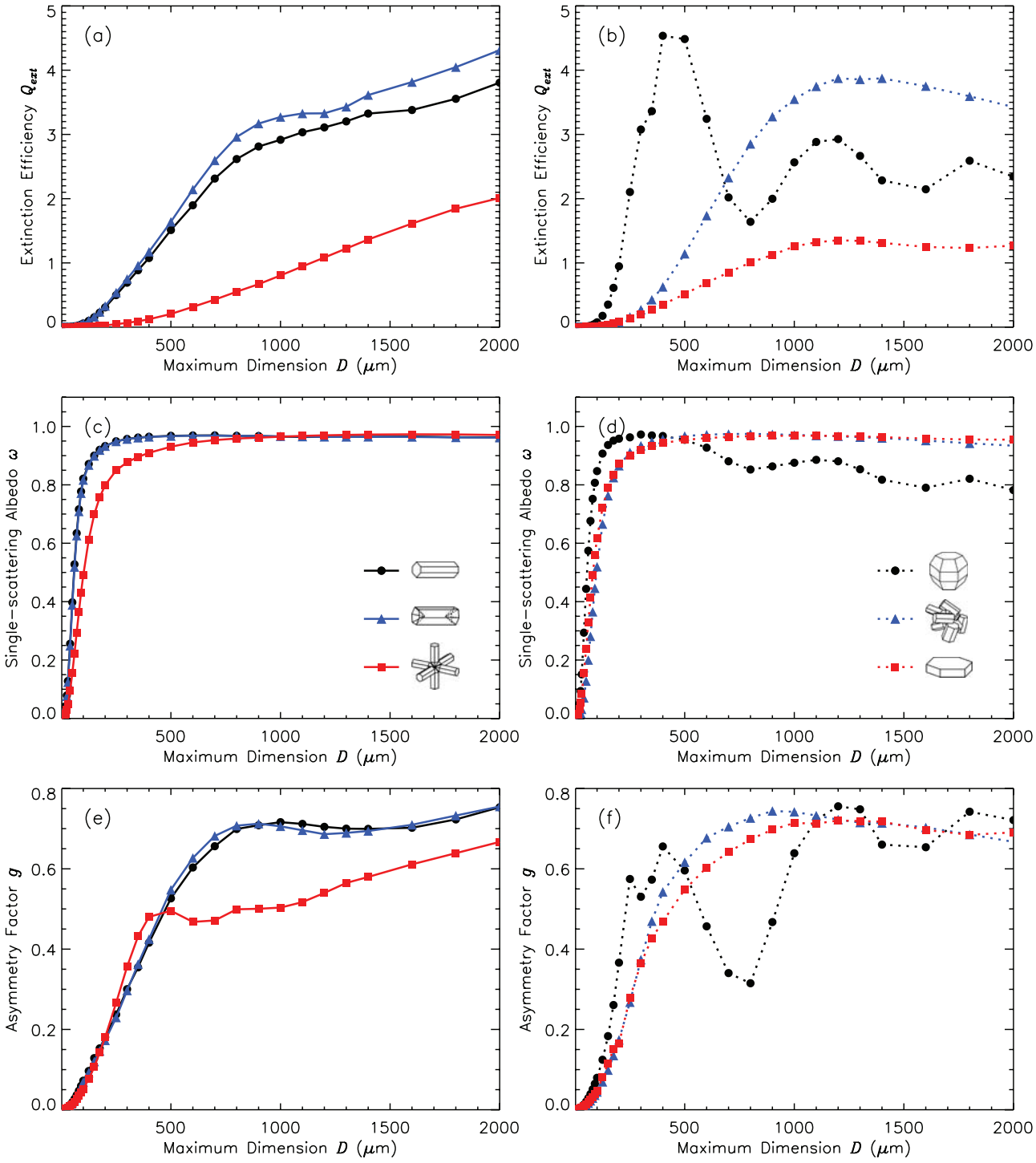

Figure 3. Extinction efficiency Q_{ext}, single-scattering albedo ω, and asymmetry factor g as a function of maximum dimension D at 640 GHz for the six nonspherical ice habits.

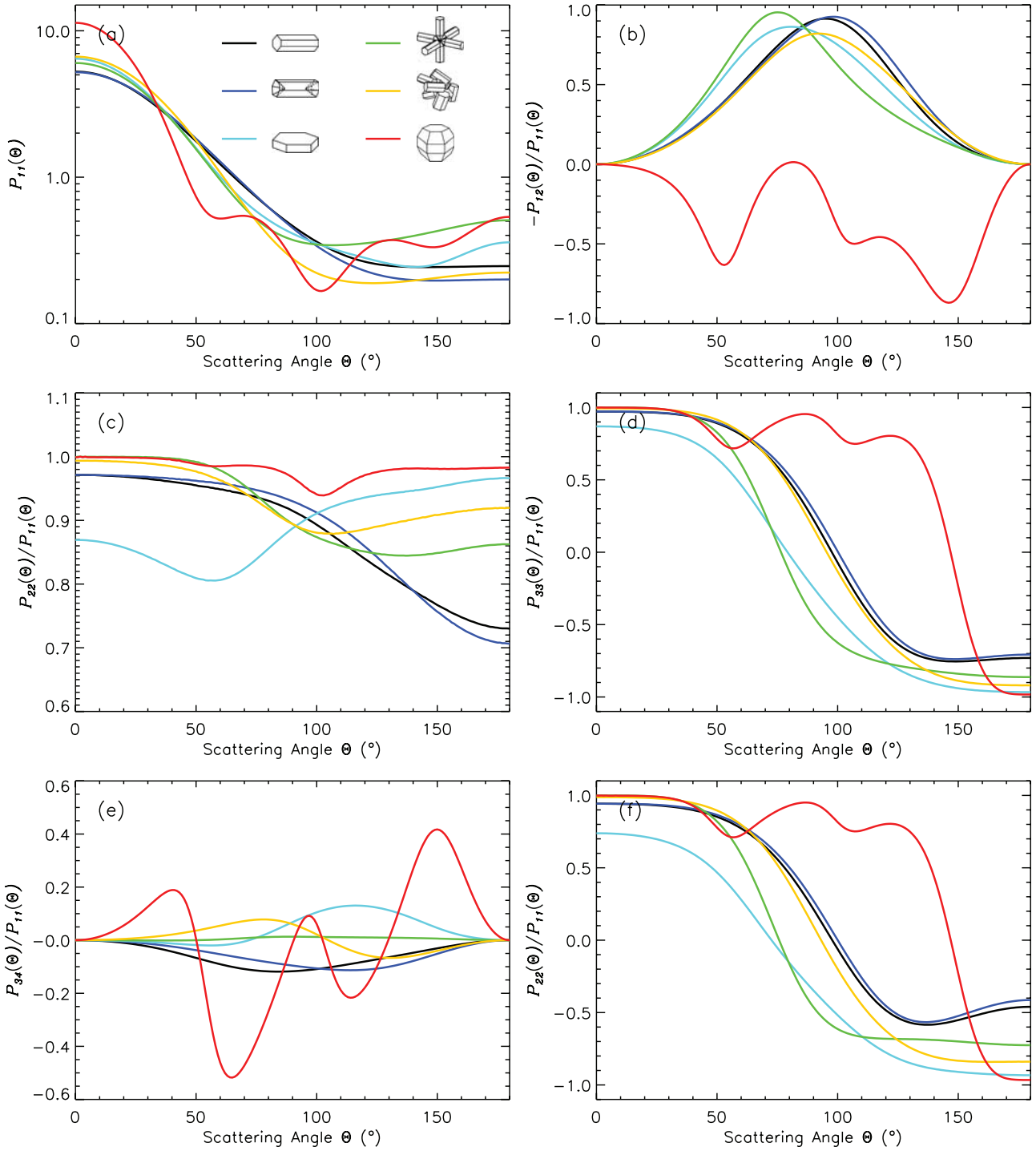

Figure 4. Scattering phase matrix elements as a function of scattering angles Θ for the six nonspherical ice habits at 640 GHz for D = 500 μm.

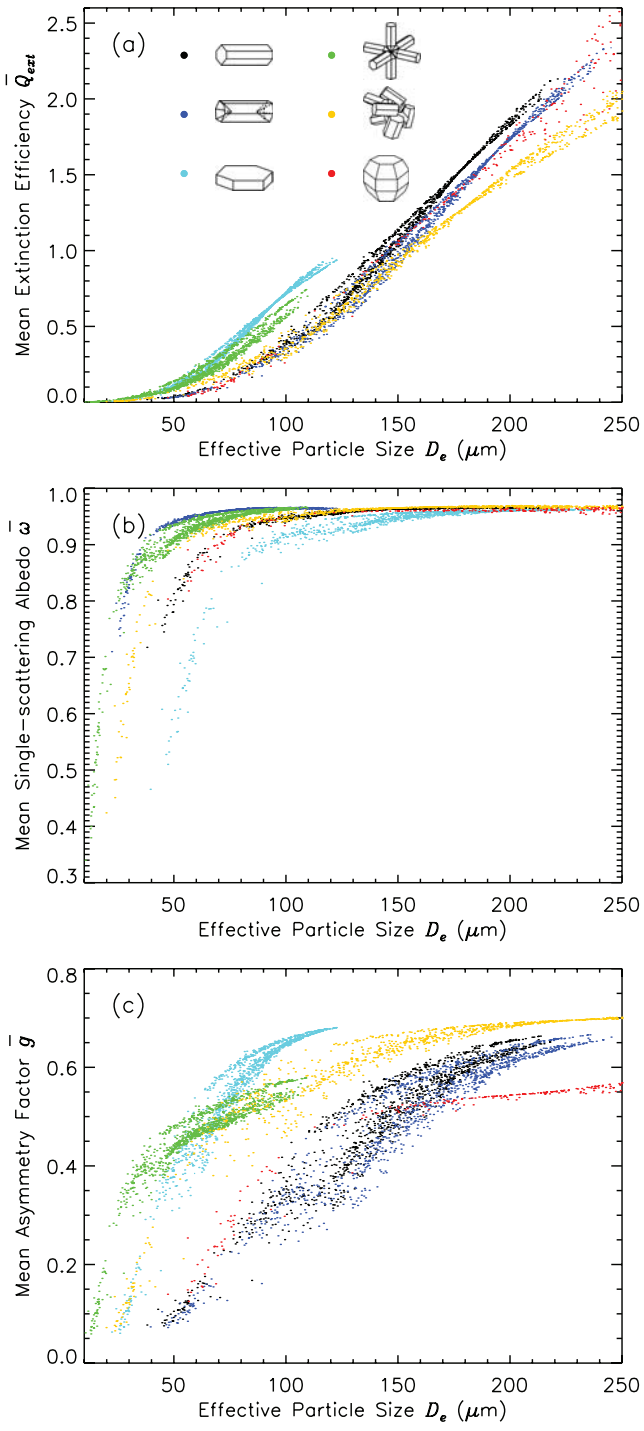

Figure 5. Mean extinction efficiency $\overline{Q}_{ext}$, mean single-scattering albedo $\overline{\omega}$, and mean asymmetry factor $\overline{g}$ as a function of effective particle size D_e at 640 GHz as calculated from in situ particle size distributions for the six nonspherical ice habits.

Wisconsin in 1986 (called FIRE-I), another FIRE campaign in Coffeyville, Kansas in 1991 (called FIRE-II), and the Atmospheric Radiative Measurement Program Intensive Operational Period (ARM-IOP) near Lamont, Oklahoma in 2000. Detailed information about the microphysical measurements is provided in *Miloshevich and Heymsfield* [1997], *Heymsfield et al.* [2002, 2003, 2004], and *Heymsfield and Miloshevich* [2003]. From a much larger set, a total of 1119 PSDs for ice clouds are chosen that are based on screening procedures discussed in *Baum et al.* [2005a].

3. Database of Scattering Properties of Ice Clouds

[14] The single-scattering properties (the extinction efficiency Q_{ext}, single-scattering albedo ω, asymmetry factor g, and the scattering phase matrix) of the six nonspherical ice particles are computed by the DDA method at 21 frequencies from 89 to 874 GHz for 38 discrete sizes ranging from 2 to 2000 μm. This set of chosen frequencies covers most current and planned near future satellite and airborne sensors are listed in Table 1. Figures 3 and 4 show examples of the single-scattering properties included in the database.

[15] Figure 3 shows Q_{ext}, ω, and g as functions of D for the six nonspherical ice habits at microwave frequency 640 GHz. In general, the single-scattering properties differ between the various habits except for hexagonal solid and hollow columns, which have similar features. In the particle size range considered in this study, pronounced oscillations of Q_{ext}, ω, and g tend to occur for droxtals at high frequencies.

[16] The complete scattering matrix is required for a vector atmospheric radiative transfer model to simulate the full four Stokes parameters [e.g., *Mishchenko et al.*, 2002, 2006; *Baran*, 2004; *Hovenier et al.*, 2004; *Kokhanovsky*, 2006]. Even though there are several radiative transfer models that can treat oriented ice particles (e.g., ARTS [*Emde et al.*, 2004]), most models assume random orientation [e.g., *Platnick et al.*, 2003; *King et al.*, 2004, 2006; *Yang et al.*, 2005; *Baum et al.*, 2005a, 2005b]. Although this assumption is not generally valid, it is for practical reasons a good starting point for a scattering database. In a case for ice particles are randomly oriented in ice clouds such that every particle has a plane of symmetry, the scattering phase matrix $\mathbf{P}(\cos\Theta)$ then has only six independent matrix nonzero elements [*van de Hulst*, 1957; *Liou*, 2002],

$$\mathbf{P}(\cos\Theta) = \begin{bmatrix} P_{11} & P_{12} & 0 & 0 \\ P_{12} & P_{22} & 0 & 0 \\ 0 & 0 & P_{33} & P_{34} \\ 0 & 0 & -P_{34} & P_{44} \end{bmatrix}. \quad (1)$$

The six independent matrix nonzero elements (P_{11}, P_{12}, P_{22}, P_{33}, P_{34}, and P_{44}) are computed at 181 scattering angle Θ in the range of 0° to 180° for each D and frequency.

[17] Figure 4 shows the six elements of the scattering phase matrix as functions of scattering angle Θ at a frequency of 640 GHz for the six habits for a D of 500 μm, which has similar features to the Q_{ext}, ω, and g shown in Figure 3. The six elements depend strongly on the habit, with the exception of hexagonal solid and hollow columns being quite similar when D is small. However, with increasing D, the six elements show distinct differences for all the six habits. The oscillations of scattering phase matrix elements become stronger as D increases (figures are not shown).

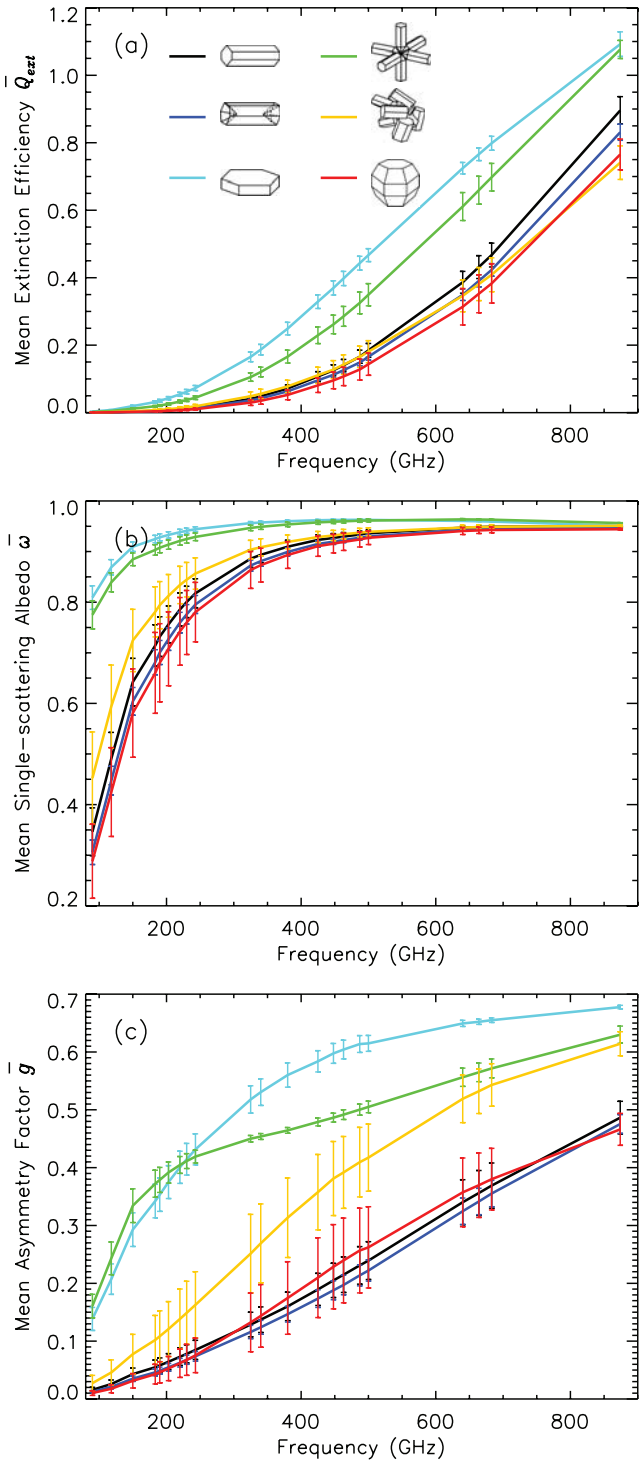

Figure 6. Mean extinction efficiency $\overline{Q}_{ext}$, mean single-scattering albedo $\overline{\omega}$, and mean asymmetry factor $\overline{g}$ as a function of frequency for the six nonspherical ice habits for D_e = 100 μm. The error bars indicate the standard deviations.

[18] To obtain bulk scattering properties that may be more representative of ice clouds, the single-scattering properties for the individual particles are integrated over the measured 1119 PSDs for an assumed habit mixture. The effective particle size D_e [e.g., *Foot*, 1988; *King et al.*, 2004; *Yang et al.*, 2005; *Baum et al.*, 2005b] is computed by:

$$D_e = \frac{3}{2}\frac{\int_{D_{\min}}^{D_{\max}}\left[\sum_{i=1}^{N} f_i(D)V_i(D)\right]N(D)\mathrm{d}D}{\int_{D_{\min}}^{D_{\max}}\left[\sum_{i=1}^{N} f_i(D)S_i(D)\right]N(D)\mathrm{d}D}, \quad (2)$$

where $N(D)$ is the number density of ice particle with a D, $\sum_{i=1}^{N} f_i(D) = 1$, $f_i(D)$ is the ice particle habit percentage for habit i at a D for up to N habits, $V_i(D)$ and $S_i(D)$ are the volume and project area of the habit i for a given D, respectively, and $D_{\min}$ and $D_{\max}$ are the minimum and maximum sizes of D in the given $N(D)$, respectively.

[19] The bulk scattering properties (the mean extinction efficiency $\overline{Q}_{ext}$, mean single-scattering albedo $\overline{\omega}$, mean asymmetry factor $\overline{g}$, and mean scattering phase matrix elements $\overline{P}_{11}$, $\overline{P}_{12}$, $\overline{P}_{22}$, $\overline{P}_{33}$, $\overline{P}_{34}$, and $\overline{P}_{44}$) of ice clouds are computed using the same method as *Yang et al.* [2005], *Baum et al.* [2005b], and *Hong* [2007a].

[20] Bulk ice cloud scattering properties are first developed assuming that the cloud is composed of a single habit (i.e., $N = 1$ in equation (2)) since insufficient information on ice habits and their typical percentages for any given size distribution [*King et al.*, 2004; *Yang et al.*, 2005]. For these clouds composed of a single habit, the $\overline{Q}_{ext}$, $\overline{\omega}$, and $\overline{g}$ for ice clouds are shown in Figure 5 at a frequency of 640 GHz. The range of D_e ranges from 10 to 250 μm. The minima and maxima of D_e are different for the six habits. The $\overline{Q}_{ext}$ and $\overline{g}$ increase monotonically with increasing D_e for all habits in the size range. The $\overline{\omega}$ initially increases with D_e, and then tends to reach their asymptotic values as D_e passes a threshold that varies with habits. The variations of $\overline{g}$ vary with D_e for all habits. Generally the variations are stronger when D_e is in the range of small to medium size ranges with respect to their large sizes for each habit.

[21] Based on a set of the 1119 PSDs, the bulk scattering properties are developed for a defined set of D_e in the range of 50–200 μm for solid columns and droxtals, 40–200 μm for hollow columns and aggregates, 30–120 μm for plates, and 20–100 μm for bullet rosettes in increments of 10 μm [*Baum et al.*, 2005b, 2007]. The different ranges of D_e for each habit are defined by the calculated results from the PSDs because of their different geometries. The mean scattering properties at each defined D_e are obtained by averaging the individual models that fall within ±2 μm of the defined D_e. The standard deviations of the bulk scattering properties for each D_e are also computed. The calculated standard deviations can be used to estimate retrieval errors [*Baum et al.*, 2005b].

[22] Figure 6 shows the $\overline{Q}_{ext}$, $\overline{\omega}$, and $\overline{g}$ for ice clouds composed of each of the six habits at D_e = 100 μm for all 21 frequencies considered in this study. The standard deviations are also shown by error bars. The variations of $\overline{Q}_{ext}$, $\overline{\omega}$, and $\overline{g}$ with frequencies are similar to the variations with D shown in Figure 5. Both $\overline{Q}_{ext}$ and $\overline{g}$ increase monotonically with frequency for all habits. The $\overline{\omega}$ increases with frequency until it reaches its asymptotic value, which is about 250 GHz for plates and bullet rosettes and about

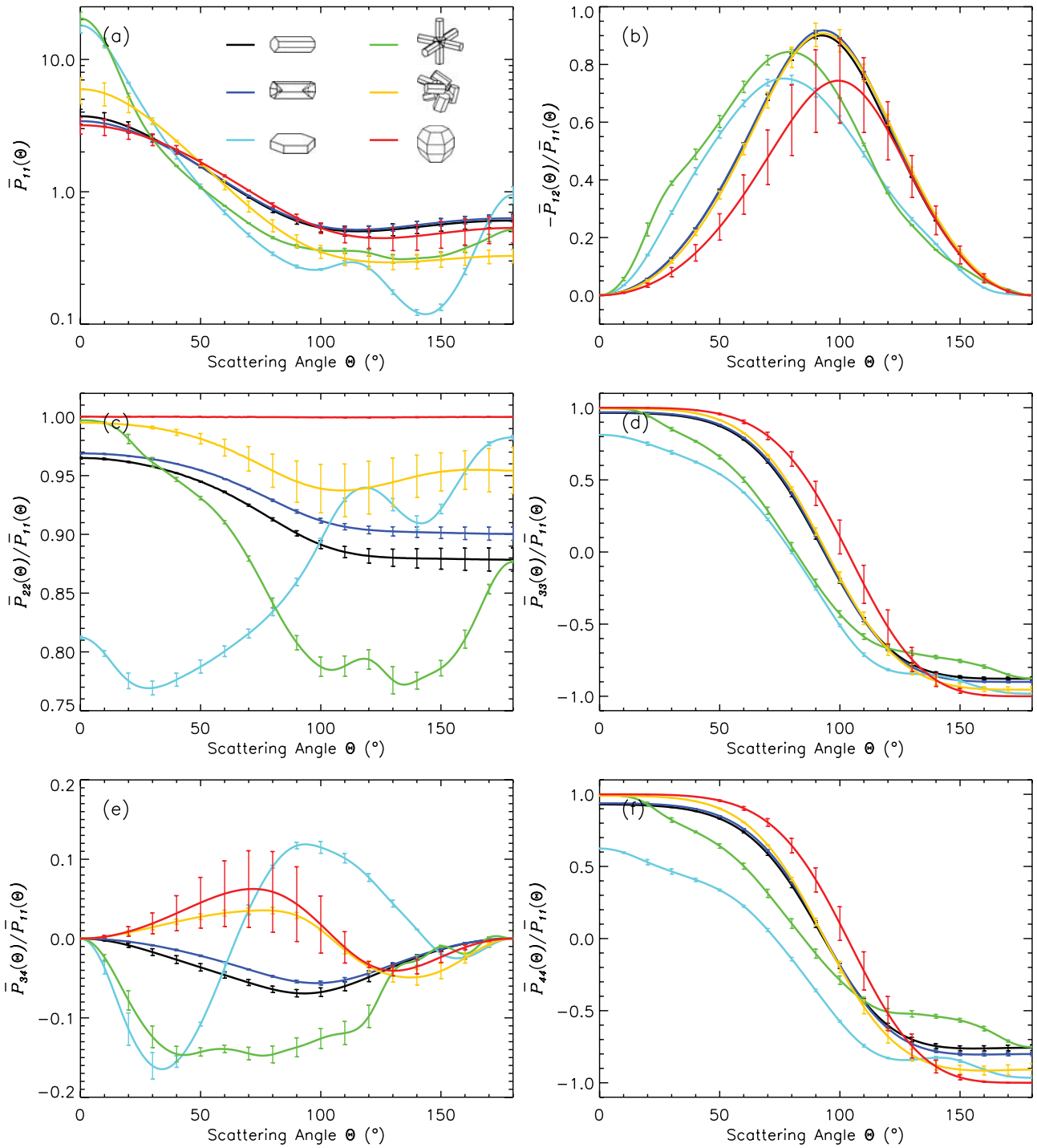

Figure 7. Mean scattering phase matrix elements a function of scattering angles Θ at 640 GHz for the six nonspherical ice habits for D_e = 100 μm. The error bars indicate the standard deviations.

450 GHz for solid and hollow columns, aggregates, and droxtals. Solid and hollow columns, aggregates, and droxtals have similar values of $\overline{Q}_{ext}$ and $\overline{\omega}$ for a given frequency while plates and bullet rosettes have similar values. Solid and hollow columns and droxtals have similar values of $\overline{g}$. The $\overline{\omega}$ and $\overline{g}$ for aggregates and droxtals have large standard deviations.

[23] The mean scattering phase matrix elements $\overline{P}_{11}$, $\overline{P}_{12}$, $\overline{P}_{22}$, $\overline{P}_{33}$, $\overline{P}_{34}$, and $\overline{P}_{44}$ for ice clouds composed solely of an individual habit at D_e = 100 μm are shown in Figure 7 at 640 GHz. Droxtals have large deviations for the mean scattering phase matrix elements except for $\overline{P}_{22}$, for which aggregates display the largest deviations.

[24] The previous results assumed that the ice clouds were composed of a single habit. It is more sensible to adopt a habit mixture [e.g., *Yang et al.*, 2005, 2007; *Baum et al.*, 2005b; *King et al.*, 2004, 2006]. *Baum et al.* [2005a] developed one possible habit mixture based on D: D < 60 μm, 100%

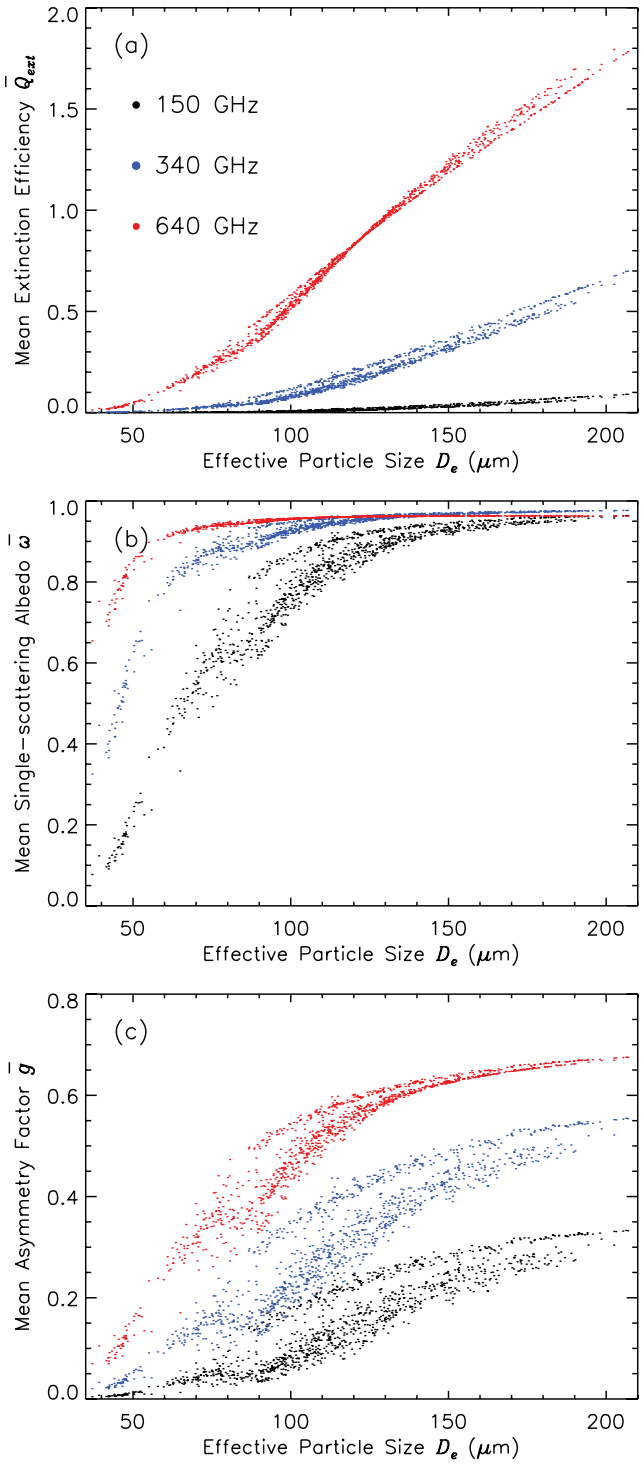

Figure 8. Mean extinction efficiency $\overline{Q}_{ext}$, mean single-scattering albedo $\overline{\omega}$, and mean asymmetry factor $\overline{g}$ as a function of effective particle size D_e calculated from in situ particle size distributions for the ice clouds with a mixture of six nonspherical ice habits at frequencies of 150, 340, and 640 GHz.

droxtals; 60 μm < D < 1000 μm, 15% bullet rosettes, 50% solid columns, and 35% plates; 1000 μm < D < 2500 μm, 45% hollow columns, 45% solid columns, and 10% aggregates; D > 2500 μm, 97% bullet rosettes and 3% aggregates.

This habit distribution was used to develop models that are adopted in MODIS Collection 5 [*King et al.*, 2006] retrievals of optical thickness and effective particle size. In this study, we also use this ice particle habit distribution to derive the bulk scattering properties of ice clouds, which are

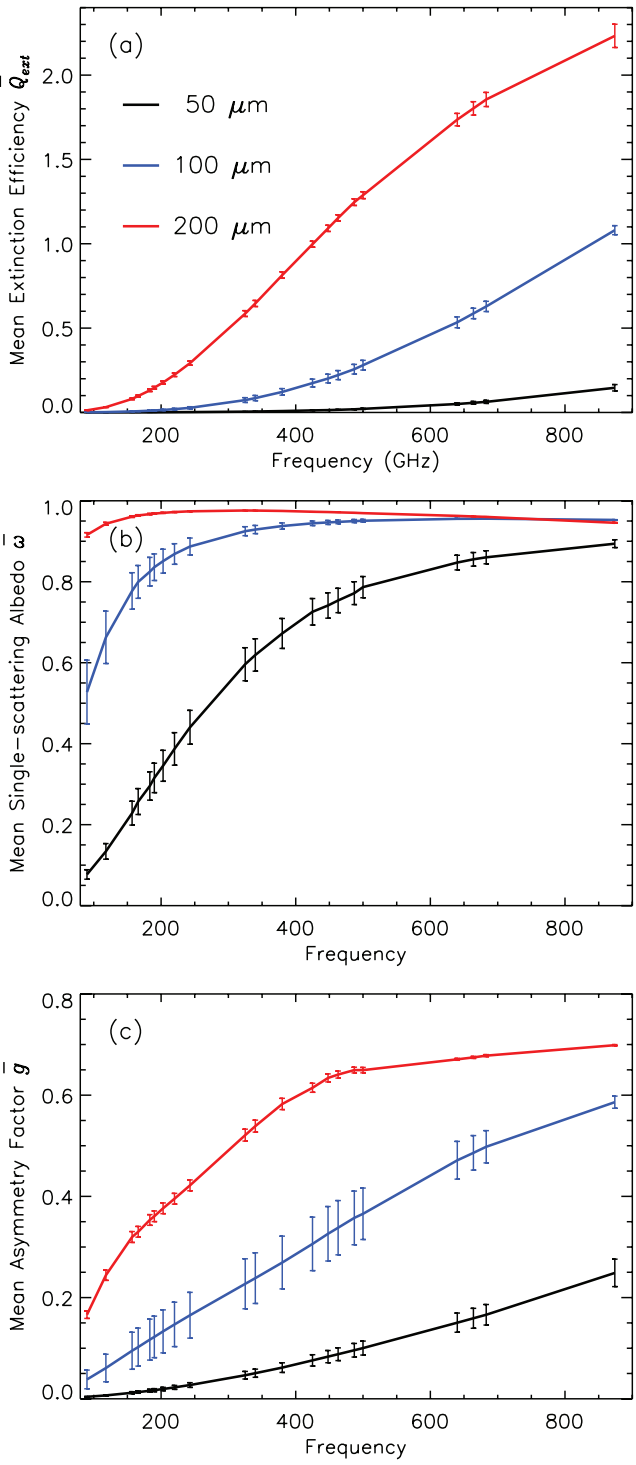

Figure 9. Mean extinction efficiency $\overline{Q}_{ext}$, mean single-scattering albedo $\overline{\omega}$, and mean asymmetry factor $\overline{g}$ as a function of frequency for the ice clouds composed of a habit mixture for D_e = 50, 100, and 200 μm. The error bars indicate the standard deviations.

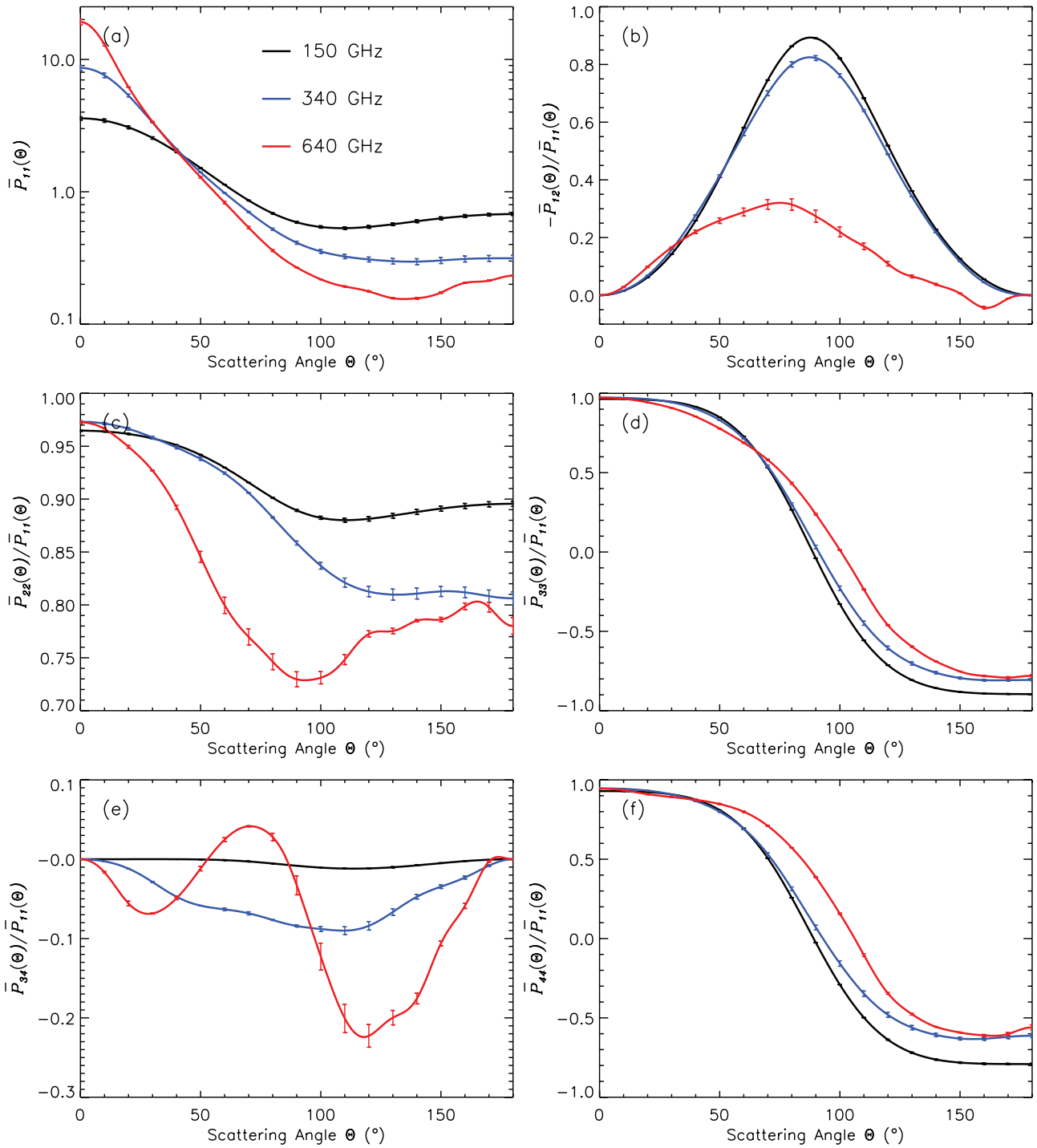

Figure 10. Mean scattering phase matrix elements at the frequencies 150, 340, and 640 GHz as a function of scattering angles for the ice clouds composed of a habit mixture for D_e = 200 μm. The error bars indicate the standard deviations.

consistent with the habit mixtures used for ice cloud retrievals in MODIS Collection 5, at millimeter and submillimeter wave frequencies.

[25] Figure 8 shows the $\overline{Q}_{ext}$, $\overline{\omega}$, and $\overline{g}$ for the 1119 ice clouds composed of the above habit mixture at frequencies of 150, 340, and 640 GHz. The $\overline{Q}_{ext}$ and $\overline{g}$ increase monotonically with D_e, for all frequencies. The $\overline{\omega}$ also increase with D_e until the asymptotic value is reached. The $\overline{\omega}$ at high frequencies increases faster than those at low frequencies. The $\overline{\omega}$ reach their asymptotic values at D_e = 80, 120, and 160 μm for the frequencies 150, 340, and 640 GHz, respectively. For a given D_e, the $\overline{g}$ show large variations with respect to the $\overline{Q}_{ext}$ and $\overline{\omega}$. The results for Figures 6 and 7, developed assuming a single habit, are extended by adopting a habit mixture with results shown in Figure 9. Figure 9 shows the $\overline{Q}_{ext}$, $\overline{\omega}$, and $\overline{g}$ at the 21

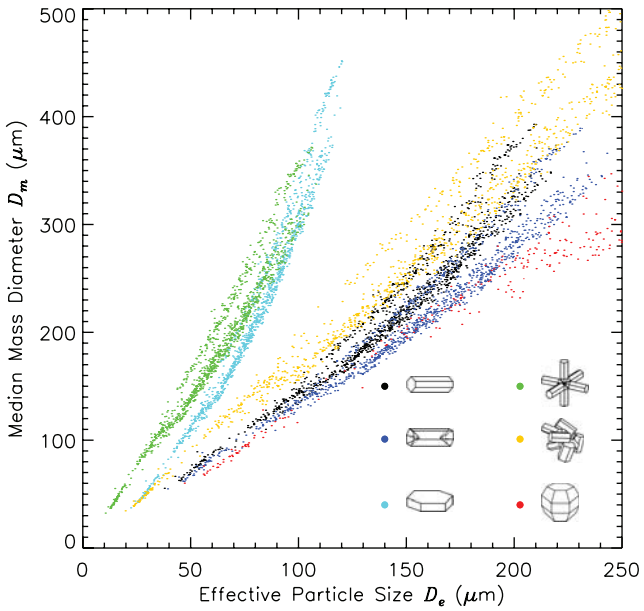

Figure 11. Relationships between the D_e and the D_m for each habit.

frequencies for D_e = 50, 100, and 200 μm, respectively. The $\overline{Q}_{ext}$ and $\overline{g}$ increase with frequency and D_e. Moreover, the $\overline{Q}_{ext}$ have stronger sensitivity to frequencies for larger D_e. When D_e = 200 μm, the $\overline{\omega}$ values are around 0.95 while those for smaller D_e increase with frequencies and tend to reach their asymptotic value. In general, the pronounced deviations are found only for $\overline{\omega}$ and $\overline{g}$ when D_e = 50 and 100 μm. The mean scattering phase matrix elements ($\overline{P}_{11}$, $\overline{P}_{12}$, $\overline{P}_{22}$, $\overline{P}_{33}$, $\overline{P}_{34}$, and $\overline{P}_{44}$) for ice clouds composed of the habit mixture vary with D_e. For small D_e (figures are not shown) the mean scattering phase matrix elements at these frequencies show similar trends, particularly for $\overline{P}_{12}$, $\overline{P}_{33}$, and $\overline{P}_{44}$ which have close values. Distinct deviations are only found for $\overline{P}_{22}$ at these frequencies. The differences of the mean scattering phase matrix elements at these frequencies increase with D_e. Figure 10 shows the mean scattering phase matrix elements for D_e = 200 μm at the three frequencies 150, 340, and 640 GHz.

[26] The D_e is often used for visible and infrared wavelength radiative transfer calculations while the median mass equivalent diameter (D_m), which characterizes the mass-weighted size of particle size distribution, is often used for radiative transfer calculations at millimeter and submillimeter-wave frequencies [e.g., *Evans et al.*, 1998, 2005; *Buehler et al.*, 2007]. The D_m is defined as the size that divides the mass content of a particle size distribution in half, i.e., the total mass of the particles with smaller sizes than D_m is equal to that with larger sizes than D_m. Figure 11 shows the relationships between the D_m and the D_e for each habit. As expected, the D_m and the D_e have distinct correlations, but the D_m has larger variation ranges for each habit than those for the D_e.

[27] The $\overline{Q}_{ext}$, $\overline{\omega}$, and $\overline{g}$ for ice clouds composed of a single habit are shown in Figure 12 at a frequency of 640 GHz in the range of D_m from 50 to 500 μm. The variations of $\overline{Q}_{ext}$, $\overline{\omega}$, and $\overline{g}$ with the D_m are similar to those shown for the D_e (Figure 6). The sensitivity of the bulk scattering properties to habits are evident, particularly for the $\overline{Q}_{ext}$. However, the $\overline{\omega}$, and $\overline{g}$ with the D_m show less sensitivity to habits than those with the D_e. Moreover, the D_m has similar size ranges for each habit, which is also shown in Figure 11. These features confirm that that the D_m is indeed a potentially better choice to characterize size information of ice clouds for microwave remote sensing as

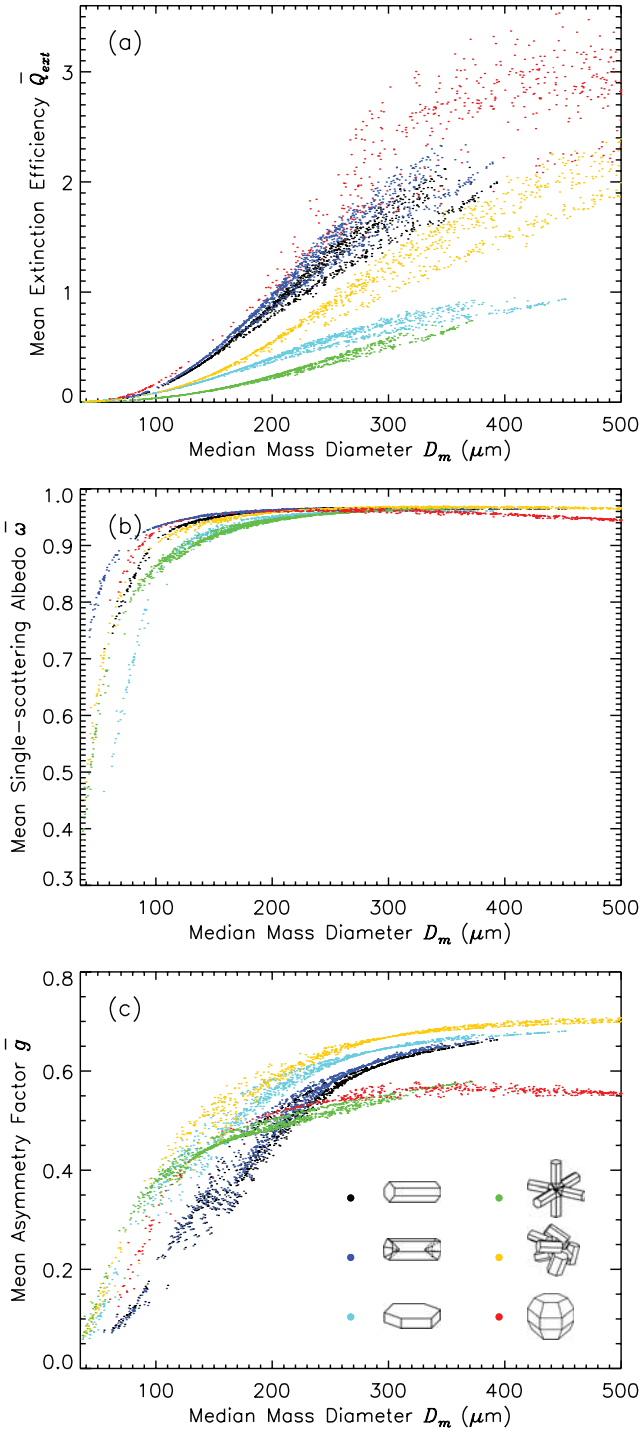

Figure 12. Mean extinction efficiency $\overline{Q}_{ext}$, mean single-scattering albedo $\overline{\omega}$, and mean asymmetry factor $\overline{g}$ as a function of mass equivalent diameter D_m at 640 GHz as calculated from in situ particle size distributions for the six nonspherical ice habits.

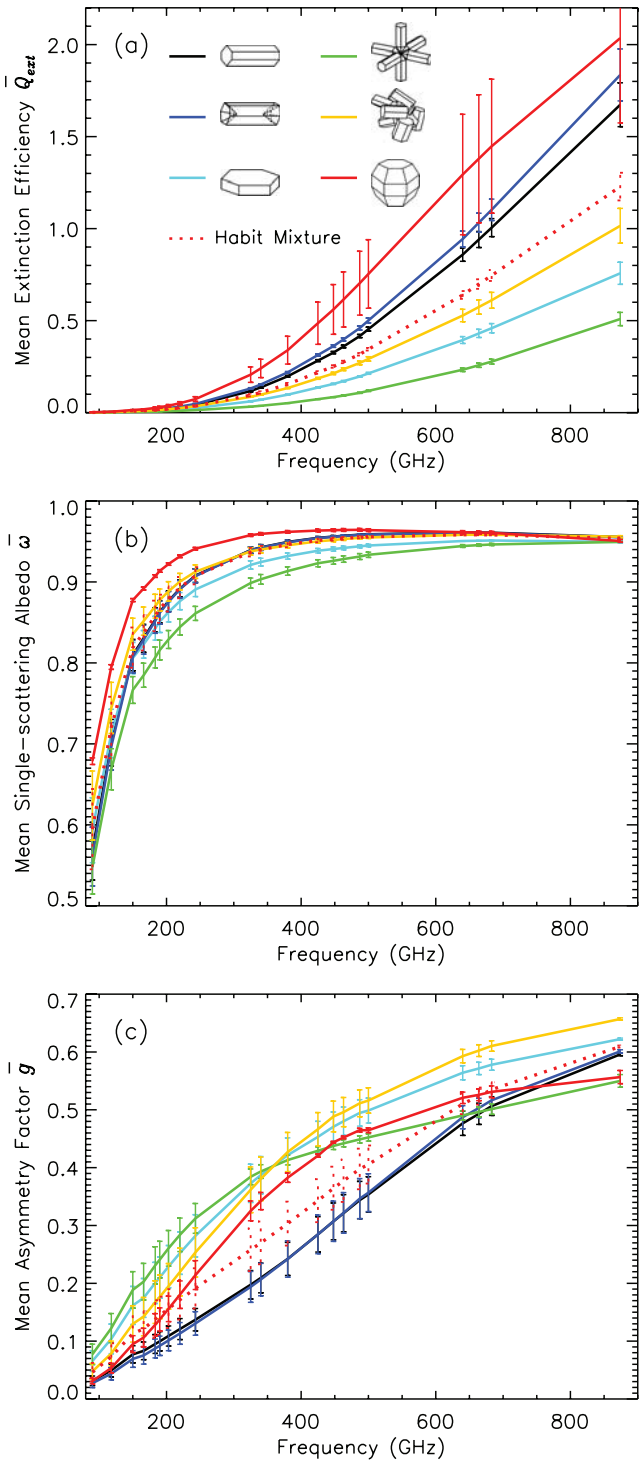

Figure 13. Mean extinction efficiency $\overline{Q}_{ext}$, mean single-scattering albedo $\overline{\omega}$, and mean asymmetry factor $\overline{g}$ as a function of frequency for the six nonspherical ice habits and a habit mixture for the median mass equivalent diameter D_m = 200 μm. The error bars indicate the standard deviations.

assumed by *Evans et al.* [1998, 2005] and *Buehler et al.* [2007].

[28] The mean bulk scattering properties of ice clouds composed of a single habit or a habit mixture are also developed for a defined set of D_m in the range of 50–500 μm in increments of 25 μm by averaging the values of bulk scattering properties within ±2.5 μm of the defined D_m. The standard bulk scattering properties at each D_m are also computed. Figure 13 shows the $\overline{Q}_{ext}$, $\overline{\omega}$, and $\overline{g}$ for ice clouds composed of each of the six habits and of the habit mixture at D_m = 200 μm for all 21 frequencies. The error bars indicate the standard deviations. Similar to those shown in Figure 7, the mean scattering properties show pronounced dependences on habit. For a given frequency, the variation of the mean scattering properties with habit at a given D_m are significantly different from those at a given D_e. The mean scattering phase matrix elements $\overline{P}_{11}$, $\overline{P}_{12}$, $\overline{P}_{22}$, $\overline{P}_{33}$, $\overline{P}_{34}$, and $\overline{P}_{44}$ for ice clouds (figures are not shown here) also show strong sensitivity of the mean phase matrix to ice particle habit.

4. Conclusions

[29] In this study, a database of the single-scattering properties (extinction efficiency, single-scattering albedo, asymmetry factor, and the full scattering phase matrix) of randomly oriented nonspherical ice particles are computed at 21 millimeter and submillimenter-wave frequencies ranging from 100 to 1000 GHz by the discrete dipole approximation (DDA) method. The ice particle habits include hexagonal solid and hollow columns, hexagonal plates, and 3D bullet rosettes, aggregates, and droxtals. The 21 millimeter and submillimeter-wave frequencies include those in most current and planned near future satellite and airborne sensors. The calculations are performed at 38 ice particle sizes based on the maximum dimension, and ranges from 2 to 2000 μm. The influence of ice habit on the single-scattering properties is investigated. The dependence of the single-scattering properties on the particle maximum dimension and millimeter and submillimeter-wave frequencies are discussed. The accuracy in the DDA computations is mostly due to the dipole sizes and the orientations for random orientation [e.g., *Draine and Flatau*, 1994, 2004; *Evans and Stephens*, 1995; *Liu*, 2004, 2008; *Hong*, 2007a; *Penttilä et al.*, 2007; *Yurkin et al.*, 2007a, 2007b]. The present results of single-scattering properties from the DDSCAT have reasonable accuracy because of using the conservative criterion with $|m|kd <$ 0.5 and orientations much larger than those suggested by *Penttilä et al.* [2007] through comparing discrete dipole implementations to exact techniques. Using more orientations and smaller dipoles to improve the accuracy of the DDSCAT computation will be performed by the next efforts.

[30] The single-scattering properties for individual particles are averaged over 1119 particle size distributions obtained from several field campaigns covering tropical and midlatitude regions to infer bulk scattering properties (the mean extinction efficiency, mean single-scattering albedo, mean asymmetry factor, and mean scattering phase matrix elements). Initially, the single-scattering properties are developed assuming a single habit, and then the influence of habits on the bulk scattering properties is investigated. Subsequent results are presented in which a habit mixture is assumed, following previous studies. For both cases, the bulk scattering properties (means and standard deviations) at the 21 frequencies are developed for a defined

set of effective particle sizes in the ranges of 20–200 μm in increments of 10 μm and for a defined set of median mass equivalent diameters in the ranges of 50–500 μm in increments of 25 μm. The standard deviations can be used for forward radiative transfer models to calculate the influence of the scattering property variations on simulated radiances at millimeter and submillimeter-wave frequencies. The database can be required through http://atmo.tamu.edu/profile/GHong. Specific requirements for the database are also welcome.

[31] **Acknowledgments.** The authors thank B.T. Draine and P.J. Flatau for providing their well-documented DDA. We also thank the three anonymous reviewers for their constructive comments. Ping Yang's work is supported by a National Science Foundation (NSF) grant (ATM-0239605) and the National Oceanic and Atmospheric Administration under contract DG133E07SE3473/NEED2000-7-15205.

References

Arriaga, A. (2000), Microwave Humidity Sounder (MHS) simulations with a radiative transfer model, in *Technical Department, Tech. Memo. 5*, European Organisation for the Exploitation of Meteorological Satellites.

Aumann, H. H., et al. (2003), AIRS/AMSU/HSB on the Aqua mission: Design, science objectives, data products, and processing systems, *IEEE Trans. Geosci. Remote Sens.*, *41*, 253–264.

Aydin, K., and T. M. Walsh (1999), Millimeter wave scattering from spatial and planar bullet rosettes, *IEEE Trans. Geosci. Remote Sens.*, *37*, 1138–1150.

Baran, A. J. (2004), On the scattering and absorption properties of cirrus cloud, *J. Quant. Spectrosc. Radiat. Transfer*, *89*, 17–36.

Baum, B. A., A. J. Heymsfield, P. Yang, and S. T. Bedka (2005a), Bulk scattering properties for the remote sensing of ice clouds. part I: Microphysical data and models, *J. Appl. Meteorol.*, *44*, 1885–1895.

Baum, B. A., P. Yang, A. J. Heymsfield, S. Platnick, M. D. King, Y.-X. Hu, and S. T. Bedka (2005b), Bulk scattering properties for the remote sensing of ice clouds. part II: Narrowband Models, *J. Appl. Meteorol.*, *44*, 1896–1911.

Baum, B. A., P. Yang, S. L. Nasiri, A. K. Heidinger, A. J. Heymsfield, and J. Li (2007), Bulk scattering properties for the remote sensing of ice clouds. part III: High resolution spectral models from 100 to 3250 cm^{-1}, *J. Appl. Meteorol. Clim.*, *46*, 423–434.

Bidwell, S. W., G. M. Flaming, J. F. Durning, and E. A. Smith (2005), The Global Precipitation Measurement (GPM) Microwave Imager (GMI) instrument: Role, performance, and status, in *Geoscience and Remote Sensing Symposium, IGARSS'05, Proceedings*, 2005 IEEE International, vol. 1, 4 pp., Seoul, Korea, 25–29 July.

Blackwell, W. J., J. W. Barrett, F. W. Chen, R. V. Leslie, P. W. Rosenkranz, M. J. Schwartz, and D. H. Staelin (2001), NPOESS Aircraft Sounder Testbed-Microwave (NAST-M): Instrument description and initial flight results, *IEEE Trans. Geosci. Remote Sens.*, *39*, 2444–2453.

Bohren, C. F., and D. R. Huffman (1983), *Absorption and Scattering of Light by Small Particles*, 530 pp., Wiley, New York.

Bommarito, J. (1993), Special sensor microwave imager sounder, *Proc. SPIE*, *1935*, 230–238.

Buehler, S. A., et al. (2007), A concept for a satellite mission to measure cloud ice water path and ice particle size, *Q. J. R. Meteorol. Soc.*, *133*, 109–128.

Chauhan, N. S., D. B. Kunkee, and M. Bahrain (2005), NPOESS Conical Microwave Imager/Sounder: Warm load calibration issues and progress, in *Geoscience and Remote Sensing Symposium, IGARSS'05, Proceedings*, 2005 IEEE International, vol. 1, 2 pp., Seoul, Korea, 25–29 July.

Czekala, H., and C. Simmer (1998), Microwave radiative transfer with nonspherical precipitating hydrometeors, *J. Quant. Spectrosc. Radiat. Transfer*, *60*, 365–374.

Czekala, H., S. Havemann, K. Schmidt, T. Rother, and C. Simmer (1999), Comparison of microwave radiative transfer calculations obtained with three different approximations of hydrometeor shape, *J. Quant. Spectrosc. Radiat. Transfer*, *63*, 545–558.

Desbois, M., R. Roca, L. Eymard, N. Viltard, M. Viollier, J. Srinivasan, and S. Narayanan (2003), The Megha-Tropiques mission, *Proc. SPIE*, *4899*, 172–183, April.

Draine, B. T., and P. J. Flatau (1994), Discrete-dipole approximation for scattering calculations, *J. Opt. Soc. Am. A Opt. Image Sci.*, *11*, 1491–1499.

Draine, B. T., and P. J. Flatau (2004), *User Guide to the Discrete Dipole Approximation Code DDSCAT 6.1*. (Available at http://arxiv.org/abs/astro-ph/0409262v2)

Emde, C., S. A. Buehler, C. Davis, P. Eriksson, T. R. Sreerekha, and C. Teichmann (2004), A polarized discrete ordinate scattering model for simulations of limb and nadir longwave measurements in 1–D/3–D spherical atmospheres, *J. Geophys. Res.*, *109*, D24207, doi:10.1029/2004JD005140.

Eriksson, P., M. Ekström, B. Rydberg, and D. P. Murtagh (2007), First Odin sub-mm retrievals in the tropical upper troposphere: ice cloud properties, *Atmos. Chem. Phys.*, *7*, 471–483.

Evans, K. F., and G. L. Stephens (1995), Microwave radiative transfer through clouds composed of realistically shaped ice crystals. part I: Single scattering properties, *J. Atmos. Sci.*, *52*, 2041–2057.

Evans, K. F., S. J. Walter, A. J. Heymsfield, and M. N. Deeter (1998), Modeling of submillimeter passive remote sensing of cirrus clouds, *J. Appl. Meteorol.*, *37*, 184–205.

Evans, K. F., S. J. Walter, A. J. Heymsfield, and G. M. McFarquhar (2002), The Submillimeter-wave cloud ice radiometer: Simulations of retrieval algorithm performance, *J. Geophys. Res.*, *107*(D3), 4028, doi:10.1029/2001JD000709.

Evans, K. F., J. R. Wang, P. E. Racette, G. Heymsfield, and L. Li (2005), Ice cloud retrievals and analysis with the Compact Scanning Submillimeter Imaging Radiometer and the Cloud Radar System during CRYSTAL FACE, *J. Appl. Meteorol.*, *44*, 839–859.

Falcone, V. J., et al. (1992), DMSP F-11 SSM/T2 calibration and validation data analysis, *Philips Laboratory Rep. PL-TR-92-2293*, Hanscom AFB, 108 pp.

Foot, J. S. (1988), Some observations of the optical properties of clouds. part II: Cirrus, *Quart. J. Roy. Meteorol. Soc.*, *114*, 145–164.

Heymsfield, A. J., and L. M. Miloshevich (2003), Parameterization for the cross-sectional area and extinction of cirrus and stratiform ice cloud particles, *J. Atmos. Sci.*, *60*, 936–956.

Heymsfield, A. J., A. Bansemer, P. R. Field, S. L. Durden, J. Stith, J. E. Dye, W. Hall, and T. Grainger (2002), Observations and parameterizations of particle size distributions in deep tropical cirrus and stratiform precipitating clouds: Results from in situ observations in TRMM field campaigns, *J. Atmos. Sci.*, *59*, 3457–3491.

Heymsfield, A. J., S. Matrosov, and B. A. Baum (2003), Ice water path-optical depth relationships for cirrus and precipitating cloud layers, *J. Appl. Meteorol.*, *42*, 1369–1390.

Heymsfield, A. J., A. Bansemer, C. Schmitt, C. Twohy, and M. R. Poellot (2004), Effective ice particle densities derived from aircraft data, *J. Atmos. Sci.*, *61*, 982–1003.

Hong, G. (2007a), Parameterization of scattering and absorption properties of nonspherical ice crystals at microwave frequencies, *J. Geophys. Res.*, *112*, D11208, doi:10.1029/2006JD008364.

Hong, G. (2007b), Radar backscattering properties of nonsperhical ice crystals at 94 GHz, *J. Geophys. Res.*, *112*, D22203, doi:10.1029/2007JD008839.

Hong, G., G. Heygster, J. Notholt, and S. A. Buehler (2008a), Interannual to diurnal variations in tropical and subtropical deep convective clouds and convective overshooting from seven years of AMSU-B measurements, *J. Clim.*, *21*, 4168–4189.

Hong, G., P. Yang, B. A. Baum, and A. J. Heymsfield (2008b), Relationship between ice water content and equivalent radar reflectivity for clouds consisting of nonspherical ice particles, *J. Geophys. Res.*, *113*, D20205, doi:10.1029/2008JD009890.

Hovenier, J. W., H. C. van de Hulst, and C. V. M. van der Mee (1986), Conditions for the elements of the scattering matrix, *Astron. Astrophys.*, *157*, 301–310.

Hovenier, J. W., H. C. van de Hulst, and H. Domke (2004), *Transfer of Polarized Light in Planetary Atmospheres: Basic Concepts and Practical Methods*, 258 pp., Kluwer Acad., Dordrecht, Netherlands.

Huang, H.-L., L. E. Gumley, K. Strabala, J. Li, E. Weisz, T. Rink, K. Bagget, J. Davies, W. L. Smith, and J. C. Dodge (2004), International MODIS and AIRS Processing Package (IMAPP): A direct broadcast software for the NASA Earth Observing System, *Bull. Am. Meteorol. Soc.*, *85*, 159–161.

Kahn, B. H., E. Fishbein, S. L. Nasiri, A. Eldering, E. J. Fetzer, M. J. Garay, and S.-Y. Lee (2007), A radiative consistency check of Atmospheric Infrared Sounder and Moderate Resolution Imaging Spectroradiometer cloud retrievals, *J. Geophys. Res.*, *112*, D09201, doi:10.1029/2006JD007486.

Kim, M.-J. (2006), Single scattering parameters of randomly oriented snow particles at microwave frequencies, *J. Geophys. Res.*, *111*, D14201, doi:10.1029/2005JD006892.

King, M. D., W. P. Menzel, Y. J. Kaufman, D. Tanré, B.-C. Gao, S. Platnick, S. A. Ackerman, L. A. Remer, R. Pincus, and P. A. Hubanks (2003), Cloud and aerosol properties, precipitable water, and profiles of temperature and humidity from MODIS, *IEEE Trans. Geosci. Remote Sens.*, *41*, 442–458.

King, M. D., S. Platnick, P. Yang, G. T. Arnold, M. A. Gray, J. C. Riédi, S. A. Ackerman, and K. N. Liou (2004), Remote sensing of liquid water

and ice cloud optical thickness, and effective radius in the arctic: Application of airborne multispectral MAS data, *J. Atmos. Ocean. Technol.*, *21*, 857–875.

King, M. D., S. Platnick, P. A. Hubanks, G. T. Arnold, E. G. Moody, G. Wind, and B. Wind (2006), *Collection 005 Change Summary for the MODIS Cloud Optical Property (06_OD) Algorithm*.

Kokhanovsky, A. A. (Ed.) (2006), *Light Scattering Reviews: Single and Multiple Light Scattering*, 493 pp., Springer, U. K.

Kunzi, K. (2001), *Cloud Ice Water Sub-millimetre Imaging Radiometer (CIWSIR): Proposal in Response to the Second Call for Proposals for Earth Explorer Opportunity Missions*, University of Bremen. (Available at http://www.iup.uni-bremen.de/iupage/psa/documents/CISWIR_proposal_final.pdf)

Lemke, H. M., and M. Quante (1999), Backscatter characteristics of nonspherical ice crystals: Assessing the potential of polarimetric radar measurements, *J. Geophys. Res.*, *104*, 31,739–31,752.

Li, J., H.-L. Huang, C.-Y. Liu, E. Weisz, L. Guan, P. Yang, H. Wei, T. J. Schmit, and W. P. Menzel (2005), Retrieval of cloud microphyiscal properties from MODIS and AIRS, *J. Appl. Meteorol.*, *44*, 1526–1543.

Liou, K. N. (2002), *An Introduction to Atmospheric Radiation*, 583 pp., Acad. Press, San Diego, Calif.

Liu, G. (2004), Approximation of single scattering properties of ice and snow particles for high microwave frequencies, *J. Atmos. Sci.*, *61*, 2441–2456.

Liu, G. (2008), A database of microwave single-scattering properties for nonspherical ice particles, *Bull. Am. Meteorol. Soc.*, *89*, 1563–1570.

Menzel, W. P., R. A. Frey, H. Zhang, D. P. Wylie, C. C. Moeller, R. E. Holz, B. Maddux, B. A. Baum, K. I. Strabala, and L. E. Gumley (2008), MODIS global cloud-top pressure and amount estimation: Algorithm description and results, *J. Appl. Meteorol. Clim.*, *47*, 1175–1198.

Miao, J., K.-P. Johnsen, S. A. Buehler, and A. Kokhanovsky (2003), The potential of polarization measurements from space at mm and sub-mm wavelengths for determining cirrus cloud parameters, *Atmos. Chem. Phys.*, *3*, 39–48.

Miloshevich, L. M., and A. J. Heymsfield (1997), A balloon-borne continuous cloud particle replicator for measuring vertical profiles of cloud microphysical properties: Instrument design, performance, and collection efficiency analysis, *J. Atmos. Oceanic Technol.*, *14*, 753–768.

Mishchenko, M. I., and J. W. Hovenier (1995), Depolarization of light backscattering by randomly oriented nonspherical particles, *Opt. Lett.*, *20*, 1356–1358.

Mishchenko, M. I., L. D. Travis, and A. A. Lacis (2002), *Scattering, Absorption, and Emission of Light by Small Particles*, 445 pp., Cambridge Univ. Press, New York.

Mishchenko, M. I., L. D. Travis, and A. A. Lacis (2006), *Multiple Scattering of Light by Particles: Radiative Transfer and Coherent Backscattering*, 494 pp., Cambridge Univ. Press, New York.

Muth, C., P. S. Lee, J. C. Shiue, and W. A. Webb (2004), Advanced Technology Microwave Sounder on NPOESS and NPP, in *Geoscience and Remote Sensing Symposium, IGARSS'04, Proceedings*, 2004 IEEE International, vol. 4, pp. 2454–2458, Anchorage, Alaska, 20–24 Sept.

Okamoto, H. (2002), Information content of the 95 GHz cloud radar signals: Theoretical assessment of effects of non-sphericity and error evaluations of the discrete dipole approximation, *J. Geophys. Res.*, *107*(D22), 4628, doi:10.1029/2001JD001386.

Penttilä, A., E. Zubko, K. Lumme, K. Muinonen, M. A. Yurkin, B. Draine, J. Rahola, A. G. Hoekstra, and Y. Shkuratov (2007), Comparison between discrete dipole implementations and exact techniques, *J. Quant. Spectrosc. Radiat. Transfer*, *106*, 417–436.

Piepmeier, J. R., and A. J. Gasiewski (1996), Polarimetric Scanning Radiometer for airborne microwave imaging studies, in *Proceedings of the 1996 International Geoscience and Remote Sensing Symposium*, pp. 1688–1691, IEEE Int., Lincoln, Nebr., 27–31 May.

Platnick, S., M. D. King, S. A. Ackerman, W. P. Menzel, B. A. Baum, J. C. Riédi, and R. A. Frey (2003), The MODIS cloud products: Algorithms and examples from Terra, *IEEE Trans. Geosci. Remote Sens.*, *41*, 459–473.

Purcell, E. M., and C. R. Pennypacker (1973), Scattering and absorption of light by non-spherical dielectric grains, *Astrophys. J.*, *186*, 705–714.

Sato, K., and H. Okamoto (2006), Characterization of Ze and LDR of nonspherical and inhomogeneous ice particles for 95-GHz cloud radar: Its implication to microphysical retrievals, *J. Geophys. Res.*, *111*, D22213, doi:10.1029/2005JD006959.

Saunders, R. W., T. J. Hewison, S. J. Stringer, and N. C. Atkinson (1995), The radiometric characterization of AMSU-B, *IEEE Trans. Microwave Theory Tech.*, *43*, 760–771.

Skofronick-Jackson, G., A. Heymsfield, E. Holthaus, C. Albers, and M.-J. Kim (2008), Nonspherical and spherical characterization of ice in Hurricane Erin for wideband passive microwave comparisons, *J. Geophys. Res.*, *113*, D06201, doi:10.1029/2007JD008866.

Stith, J. L., J. E. Dye, A. Bansemer, A. J. Heymsfield, D. A. Grainger, W. A. Petersen, and R. Cifelli (2002), Microphysical observations of tropical clouds, *J. Appl. Meteorol.*, *41*, 97–117.

Stith, J. L., J. A. Haggerty, A. J. Heymsfield, and C. A. Grainger (2004), Microphysical characteristics of tropical updrafts in clean conditions, *J. Appl. Meteorol.*, *43*, 779–794.

Tang, C., and K. Aydin (1995), Scattering from ice crystals at 94 and 220 GHz millimeter wave frequencies, *IEEE Trans. Geosci. Remote Sens.*, *33*, 93–99.

van de Hulst, H. C. (1957), *Light Scattering by Small Particles*, 470 pp., Dover, Mineola, N. Y.

Wang, J. R., G. Liu, J. D. Spinhirne, P. Racette, and W. D. Hart (2001), Observations and retrievals of cirrus cloud parameters using multichannel millimeter-wave radiometric measurements, *J. Geophys. Res.*, *106*, 15,251–15,263.

Warren, S. G. (1984), Optical constants of ice from ultraviolet to the microwave, *Appl. Opt.*, *23*, 1206–1225.

Weinman, J. A., and M. J. Kim (2007), A simple model of the millimeter-wave scattering parameters of randomly oriented aggregates of finite cylindrical ice hydrometeors, *J. Atmos. Sci.*, *64*, 634–644.

Weng, F., L. Zhao, R. R. Ferraro, G. Poe, X. Li, and N. C. Grody (2003), Advanced microwave sounding unit cloud and precipitation algorithms, *Radio Sci.*, *38*(4), 8068, doi:10.1029/2002RS002679.

Wu, D. L., W. G. Read, A. E. Dessler, S. C. Sherwood, and J. H. Jiang (2005), UARS MLS cloud ice measurements and implications for H_2O transport near the tropopause, *J. Atmos. Sci.*, *62*, 518–530.

Wu, D. L., J. H. Jiang, and C. P. Davis (2006), EOS MLS cloud ice measurements and cloudy-sky radiative transfer model, *IEEE Trans. Geosci. Remote Sens.*, *44*, 1156–1165.

Yang, P., K. N. Liou, K. Wyser, and D. Mitchell (2000), Parameterization of the scattering and absorption properties of individual ice crystals, *J. Geophys. Res.*, *105*, 4699–4718.

Yang, P., H. Wei, H.-L. Huang, B. A. Baum, Y. X. Hu, G. W. Kattawar, M. I. Mishchenko, and Q. Fu (2005), Scattering and absorption property database for nonspherical ice particles in the near- through far-infrared spectral region, *Appl. Opt.*, *44*, 5512–5523.

Yang, P., L. Zhang, G. Hong, S. L. Nasiri, B. A. Baum, H.-L. Huang, M. D. King, and S. Platnick (2007), Differences between Collection 004 and 005 MODIS ice cloud optical/microphysical products and their impact on radiative forcing simulations, *IEEE Trans. Geosci. Remote Sens.*, *45*, 2886–2899.

Yurkin, M. A., and A. G. Hoekstra (2007), The discrete dipole approximation: An overview and recent developments, *J. Quant. Spectrosc. Radiat. Transfer*, *106*, 558–589.

Yurkin, M. A., A. G. Hoekstra, R. S. Brock, and J. Q. Lu (2007a), Systematic comparison of the discrete dipole approximation and the finite difference time domain method for large dielectric scatterers, *Opt. Express*, *15*, 17,902–17,911.

Yurkin, M. A., V. P. Maltsev, and A. G. Hoekstra (2007b), The discrete dipole approximation for simulation of light scattering by particles much larger than the wavelength, *J. Quant. Spectrosc. Radiat. Transfer*, *106*, 546–557.

Zhang, W., J. Xu, C. Dong, and J. Yang (2006), China's current and future meteorological satellite systems, *Earth Science Satellite Remote Sens.*, vol. 1, pp. 392–413, Science and Instruments, Springer, Berlin.

B. A. Baum, Space Science and Engineering Center, University of Wisconsin-Madison, 1225 West Dayton Street, Madison, WI 53706, USA.

S. A. Buehler, Department of Space Science, Lulea University of Technology, Box 812, SE-98128 Kiruna, Sweden.

G. Heygster, Institute of Environmental Physics, University of Bremen, P.O. Box 330440, D-28334 Bremen, Germany.

A. J. Heymsfield, National Center for Atmospheric Research, Boulder, CO 80307, USA.

G. Hong and P. Yang, Department of Atmospheric Sciences, Texas A&M University, TAMU 3150, College Station, TX 77843, USA. (hong@ariel.met.tamu.edu)

Q. Liu, Joint Center for Satellite Data Assimilation, NOAA NESDIS, Room 601, 5200 Auth Road, Camp Springs, MD 20746, USA.

F. Weng, Satellite Meteorology and Climatology Division, Center for Satellite Applications and Research, NOAA NESDIS, Room 712, 5200 Auth Road, Camp Springs, MD 20746, USA.